**Article:**
Kamsanam, W, Mao, X and Jaworski, AJ (2016) Thermal performance of finned-tube thermoacoustic heat exchangers in oscillatory flow conditions. International Journal of Thermal Sciences, 101. pp. 169-180. ISSN 1290-0729

https://doi.org/10.1016/j.ijthermalsci.2015.10.032

# Thermal performance of finned-tube thermoacoustic heat exchangers in oscillatory flow conditions

Wasan Kamsanam[a], Xiaoan Mao[b,*], Artur J. Jaworski[b]

[a] *Mechanical Engineering Department, School of Engineering, University of Phayao, 19 Moo 2 Tambon Maeka, Amphur Muang Phayao 56000, Tailand*
[b] *Faculty of Engineering, University of Leeds, Leeds LS2 9JT, United Kingdom*

**Abstract**

Heat exchangers play a key role in the overall performance of thermoacoustic devices. Due to the complex nature of oscillatory flows, the underlying mechanism of heat transfer in oscillatory flows is still not fully understood. This work investigates the effect of fin length and fin spacing on the thermal performance of finned-tube heat exchangers. The heat transfer rate between two finned-tube heat exchangers arranged side-by-side in an oscillatory flow was measured over a range of testing conditions. The results are presented in terms of heat transfer coefficient and heat transfer effectiveness. Comparisons are made between experimental results of this work and a number of models, such as, the Time-Average Steady-Flow Equivalent (TASFE) model, the Root Mean Square Reynolds Number (RMS-Re) model and the boundary layer conduction model, as well as several empirical correlations in literature. A new empirical correlation is proposed to be used for the prediction of thermal performance for finned-tube heat exchangers in oscillatory flows. The uncertainties associated with the measurement of heat flux are estimated.

*Keywords:* heat exchanger, oscillatory flow, thermoacoustics, thermal performance, Nusselt number, heat transfer effectiveness

## 1. Introduction

Thermoacoustic technology is based on thermoacoustic effects, whereby fluid adjacent to solid boundaries undergoes a thermodynamic cycle to either generate acoustic power from heat input or transport heat using the acoustic power supplied. In thermoacoustic heat engines, heat input is provided through hot heat exchangers in order for the engines to produce acoustic power at stacks or regenerators, and waste heat leaves the systems through ambient heat exchangers. In thermoacoustic refrigerators, heat is drawn from heat sources via cold heat exchangers, transported along stacks or regenerators, and rejected to heat sinks via ambient heat exchangers. The thermal interaction of heat exchangers with working fluids is crucial for the performance of the thermoacoustic devices.

The optimization of different parts of thermoacoustic refrigerators, including heat exchangers, in order to obtain the maximum cooling load were presented by Minner et al.[1] and Tijani et al.[2]. The distance between neighbouring fins, or the fin spacing, was suggested to be about 2 to 4 times the thermal penetration depth, in order to have effective heat transfer between heat exchangers and working fluids. The fin length was recommended not to be longer than the displacement amplitude.

Worlikar and Knio[3], Besnoin and Knio[4], and Marx and Blanc-Benon[5] numerically investigated the effect of a number of relevant parameters on the heat transfer from heat exchangers made of plate fins in oscillatory flows. These parameters in non-dimensional form include the heat exchanger length, the fin spacing and the gap between heat exchangers and plate stacks. In their numerical study of similar heat

*Corresponding author. Tel: +44 (0) 113 343 4807.
*Email address:* x.mao@leeds.ac.uk (Xiaoan Mao)

exchangers made of plate fins, Piccolo and his co-worker[6, 7, 8] introduced a model to predict the non-dimensional heat transfer coefficients, i.e. the Nusselt number and the Colburn-j factor. The validation of the model was undertaken by making a comparison to the experimental results obtained by Brewster et al.[9]. The comparison showed a discrepancy of about 20%.

Wakeland and Keolian[10] studied the heat transfer between two identical heat exchangers over a range of frequencies and displacement amplitudes. The plate fins of the heat exchangers are made out of extruded aluminum micro channels, which are essentially flat tubings with internal fins or ligaments for extra support and rounded edges. The experiment setup involved the two heat exchangers only with no stacks in between. The heat transfer performance was expressed in terms of heat transfer effectiveness (the ratio of the actual heat transfer rate to the maximum possible heat transfer rate). The correlations of the heat transfer effectiveness were established in accordance to the operating conditions: low and high displacement amplitudes. Peak et al.[11] investigated the thermal performance of a heat exchanger within a thermoacoustic refrigerator. The construction of the heat exchanger used is similar to an automotive radiator. Flat fins are brazed onto flat tubes with square edges. Correlations of the dimensionless heat transfer coefficient in terms of Colburn-j factor were developed. Subsequent investigations were conducted by Nsofor et al.[12] and Tang et al.[13]. In both experimental studies, circular heat exchangers with secondary fluids flowing along the circumference were studied. The heat exchangers have fins cut out in the central part using electrical discharge machining. Heat transfer correlations were proposed based on their experimental data. In addition, the experimental results were compared with several existing models, such as the Time-Average Steady-Flow Equivalent (TASFE) model, the Root Mean Square Raynolds Number (RMS-Re) model and the boundary layer conduction model.

As can be seen, the effect of the geometrical parameters of heat exchangers and operating conditions on the heat transfer to the oscillatory gas has been studied to some extent, but largely using the numerical approach. This is caused by the fact that it is rather impractical to have a large number of heat exchangers with different geometrical parameters for test. Furthermore, the plate fins examined in the numerical studies were often assumed to have constant wall temperature, and the effect of the oscillatory flow obstructed by the fins of finite thickness on heat transfer was neglected. These conditions are not always satisfied for heat exchangers in practical applications, which make experimental studies necessary and irreplaceable. There is a lack of information from experimental studies on the effect of geometrical parameters of heat exchangers and operating conditions on the heat transfer to the flow. In this study, the effect of the fin length and the fin spacing on the heat transfer performance of finned-tube heat exchangers in oscillatory flow conditions is investigated. The fin length and the fin spacing, in their non-dimensional forms, are varied by changing the mean pressure and the acoustic displacement amplitude. The experimental results are compared with some models and empirical correlations that are available in literature. In addition, a new correlation of the heat transfer effectiveness is proposed based on the experimental results in this work, which can be useful in the design of thermoacoustic heat exchangers for practical applications.

For heat transfer taking place in oscillatory flows, one of the important parameters is the thermal penetration depth ($\delta_\kappa$) in the working fluid, which is gas in this case. It is defined as follows

$$\delta_\kappa = \sqrt{\frac{2k}{\omega \rho_m c_p}}. \tag{1}$$

Here $k$, $\rho_m$ and $c_p$ are the thermal conductivity, the mean density and the isobaric specific heat of the working gas, respectively. $\omega$ is the angular frequency. The thermal penetration depth ($\delta_\kappa$) denotes a distance from the wall, within which heat can diffuse into the gas during a time of the order of an oscillation period. Another key parameter that influences the heat transfer is the gas displacement amplitude ($\xi_a$). It can be found using the following equation,

$$\xi_a = \frac{u_1}{\omega}, \tag{2}$$

when the acoustic oscillation in the gas can be assumed in a simple harmonic form. $u_1$ is the velocity amplitude at the chosen location in the acoustic field. In standing waves, the gas displacement amplitude

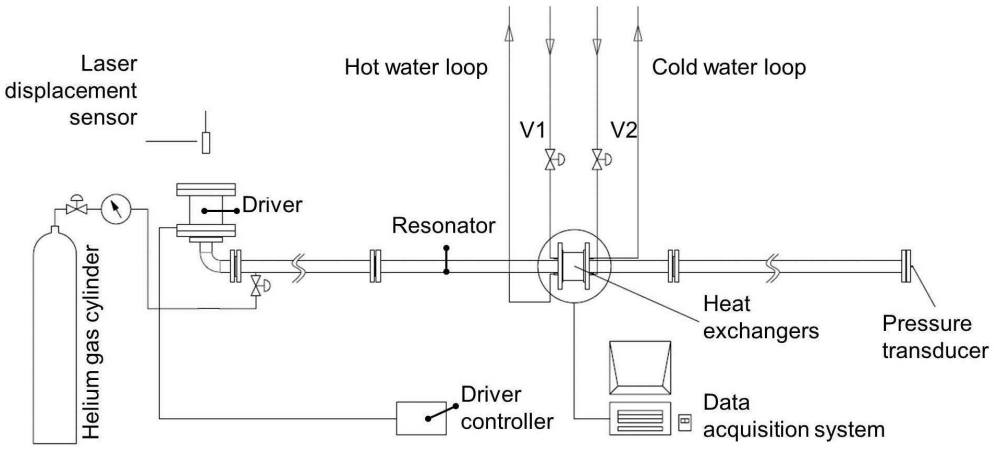


Figure 1: Schematic diagram of the experimental apparatus

($\xi_a$) can be easily obtained from the acoustic pressure amplitude using

$$\xi_a = \frac{P_a \sin(k_w x)}{\omega \rho_m a}, \tag{3}$$

where $P_a$ is the pressure amplitude measured at the acoustic pressure anti-node, $k_w (= 2\pi/\lambda)$ is the wave number with $\lambda$ being the wave length, $x$ is the distance from the pressure anti-node, and $a$ is the sound speed.

## 2. Experimental apparatus

To study the heat transfer from heat exchangers in oscillatory flows, two heat exchangers, one heated and another cooled, are placed side by side in a standing wave acoustic resonator. The resonator of a total length of 8.9 m was made of stainless steel pipes with a 52.5 mm internal diameter. Helium was used as the working gas for its popularity in thermoacoustic systems owing to its relatively low Prandtl number. The acoustic oscillation is excited by a linear electromagnetic driver mounted at one end of the resonator. The other end of the resonator is closed with a flange to make a half wavelength resonator. A schematic diagram of the experimental apparatus is shown in Fig.1. The experimental apparatus also includes a hot and a cold water circulating loops, a gas charging system and a data acquisition system. In the hot and cold water circulating loops, the water temperatures in the water bathes were kept constant using PID control.

The two heat exchanger were placed in a 100 mm long pipe with a 122 mm internal diameter, which formed the test section. This pipe and the resonator maintain the internal pressure, while the heat exchanger casings and the spacers will bear the acoustic pressure load during the tests.

In the test section, insulation was applied where applicable as shown in Fig.2. A Duratec 750® ceramic plate with a low bulk thermal conductivity ($1.46 W.m^{-1}.K^{-1}$) was used to separate the hot and cold heat exchangers. Each heat exchanger was also separated from the test section end-flanges using machined polytetrafluoroethylene (PTFE) spacers (a bulk thermal conductivity of $0.25 W.m^{-1}.K^{-1}$), to avoid a direct contact between the heat exchangers and the stainless steel flanges. Silicate wool with a thermal conductivity of $0.1 W.m^{-1}.K^{-1}$ was placed in the empty space between the heat exchangers and the stainless steel housing. The internal surface of the stainless steel pipes on both sides of the test section was lined with a polyethylene (PE) sheet of a bulk thermal conductivity of $0.5 W.m^{-1}.K^{-1}$. The thickness of the PE sheet is 1.0 mm, small enough not to cause a significant obstruction to the flow. The PE sheets are about 100 mm into the pipe measured from the flange surfaces, a length much longer than the maximum gas displacement amplitude in the current study.

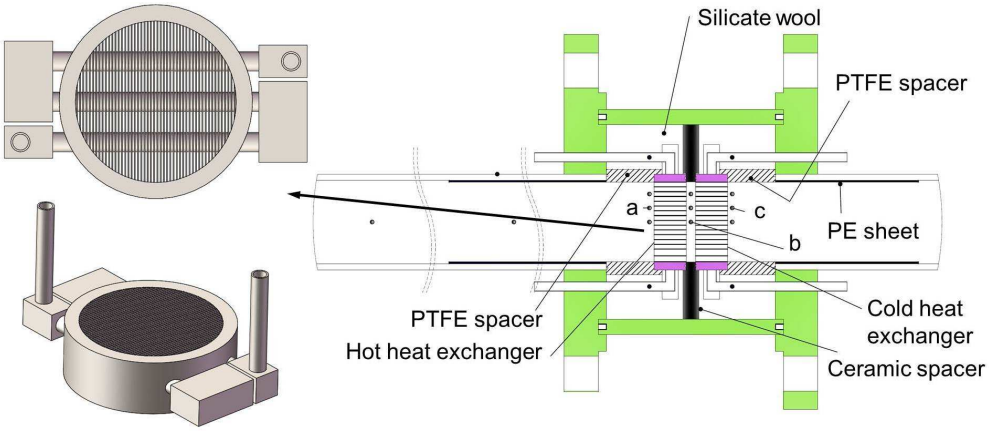


Figure 2: Construction of a finned-tube heat exchanger (left) and a cross view of the test section (right)

Table 1: Combinations of hot and cold heat exchangers

| | Fin spacing (mm) | |
|---|---|---|
| Combination | Hot heat exchanger | Cold heat exchanger |
| I | 0.7 (A) | 0.7 |
| II | 1.4 (B) | 2.1 |
| III | 2.1 (C) | 1.4 |

### *2.1. Heat exchangers*

The heat exchangers resemble the fin and tube (or finned-tube) type heat exchanger. The fins are made from 0.3 mm thick ($t$) copper sheets. Holes were drilled in each of the fins to allow three copper tubes to pass through. The tubes have 6.0 mm outer diameter and 0.5 mm wall thickness. Fins were cut to the required length and assembled with the tubes and outer copper casing, shown in Fig.2. The spacing between fins ($D$), that is, the size of the gap between any two adjacent fins, was maintained by inserts when the fins were joined to the tubes and the casing by vacuum brazing. Four heat exchangers with different fin spacing were fabricated: two heat exchangers with fin spacing of 0.7 mm (A), and one 1.4 mm (B) and one 2.1 mm (C). The fin length ($L$) along the casing axis, which is also the length of the heat exchangers, is fixed at 20 mm for all heat exchangers. As seen in Fig.2, two heat exchangers were placed at one time in the test section, one of which operates as a hot heat exchanger and another as a cold heat exchanger. The thermal performance analysis is carried out on the hot heat exchanger. The analysis on the cold heat exchanger is possible but less accurate. The flow rate of the cold water was required at a higher value. As a result, the temperature difference between the inlet and exit of the cold heat exchanger was small, leading to high uncertainty in the temperature measurement. The combinations of two heat exchangers for test are shown in Table 1. For any combination of two heat exchangers, the thermal performance of the heat exchangers determines the heat transfer rate and consequently the gas temperature in the gap between the two heat exchangers. Hence, the grouping of a cold and a hot heat exchangers can be arbitrary.

### *2.2. Measurement instrumentation*

The temperature of the working gas was collected from three locations: sections ‘a’, ‘b’ and ‘c’ as illustrated in Fig. 2. Section ‘b’ is located in the middle of the gap between the hot and cold heat exchangers. Sections ‘a’ and ‘c’ are located 3 mm away from the far sides of the two heat exchangers. At each section, three thermocouple probes were mounted, with their measuring junctions at different radial positions to obtain an averaged gas temperature in the section. The gas temperature was also recorded at 180 mm and 880 mm to the left of the hot heat exchanger in order to estimate the heat conduction in the gas. The surface temperature on the outside of the stainless steel pipe was monitored for the estimation of

the heat conduction along the pipe wall. The water temperature was measured at the inlets and exits of the hot and cold heat exchangers. Type K thermocouples were used for all the temperature measurements. The acoustic pressure in the resonator was measured by a pressure transducer (PCB Piezotronics model 112A21) at the closed end. A laser displacement sensor (Keyence model LK-G152) was used to monitor the displacement of the driver piston, through a sightglass mounted in the driver housing.

## 3. Experimental procedure

According to Minner et al.[1], Tijani et al.[2] and Swift[14], the optimal value of the fin spacing is about two to four times the thermal penetration depth ($2 \leq D/\delta_\kappa \leq 4$). Cao et al.[15] found that the heat exchanger length can be shorter than the peak-to-peak displacement amplitude when the fin spacing was relatively small in their investigated region of 1.67 - 6.67 for ($D/\delta_\kappa$). The normalized fin spacing ($D/\delta_\kappa$) in the current study is targeted to between 1.0 and 6.0 to include the optimal values. As the fin spacing is fixed for a specific heat exchanger, the thermal penetration depth is varied by changing the mean pressure. Due to the pressure rating of the experimental apparatus, the maximum $D/\delta_\kappa$ that can be achieved for heat exchangers 'A' is 3.5. While on the lower end, the minimum $D/\delta_\kappa$ is 1.5 for heat exchanger 'C', limited by the capability of the linear driver at low mean pressures. There are also a few cases when $D/\delta_\kappa$ cannot reach 1.0 for heat exchangers 'A' and 'B' .

At any part of the empty resonator, the gas displacement amplitude ($\xi_a$) is given by Eq.3. At the location of the heat exchangers, the gas displacement amplitude becomes $\xi_a/\sigma$, with $\sigma$ being the porosity of the heat exchangers, which is defined as the ratio of the cross section area of the heat exchangers open to the gas flow to the total cross section area. Because there is a small gap ($2g = 5mm$) between two heat exchangers, the *effective* dimensionless displacement amplitude is defined as $(\xi_a - g)/(\sigma L)$. In this work, $(\xi_a - g)/(\sigma L)$ is varied from -0.04, when the peak-to-peak displacement is shorter than the gap ($2g$), to 2.15 in some cases. This maximum $(\xi_a - g)/(\sigma L)$ is not always possible due to the limit in the excursion of the acoustic driver. Swift[16] recommended that heat exchangers should have a length equivalent to the peak-to-peak displacement amplitude, in order to have a big enough heat transfer area for a given flow velocity, while not a big penalty of friction loss. This corresponds to $(\xi_a - g)/(\sigma L) = 0.5$.

Once the heat exchangers were installed in the test section, the assembled resonator was vacuumized to remove the air before it was charged with helium gas. The inlet temperature of water at the hot heat exchanger was maintained constant at 40, 60 or 80 °C, while it was always kept at 22 °C at the cold heat exchanger. The mass flow rates of the hot and cold water were controlled at 1.5 and $2.5 g.s^{-1}$, respectively, determined by weighing the mass of water collected over a certain period of time.

The system mean pressure corresponds to the desired value of $D/\delta_\kappa$. The acoustic driver was set to operate at the resonance frequency to create a standing wave. The value of $(\xi_a - g)/(\sigma L)$ was varied within the range of interest by adjusting the piston displacement amplitude of the acoustic driver. Once a thermal steady state was reached, the temperature readings, the mass flow rates of the hot and cold water and the acoustic pressure amplitude were recorded, to determine the heat transfer rate between the hot and cold heat exchangers of the selected combination. The same procedure was repeated for different values of $D/\delta_\kappa$, with water at the hot heat exchanger inlet at different temperatures, for a selected pair of heat exchangers. At any test condition, the measurement was repeated three times, and the averaged values were used for subsequent analysis.

## 4. Data reduction

From the measured water temperatures and the mass flow rate, the heat transfer rate for the hot heat exchanger, $\dot{Q}$, is found on the water side according to

$$\dot{Q} = \dot{m}_w c_{p,w} (T_{w,i} - T_{w,o}). \tag{4}$$

The subscripts $w$, $i$ and $o$ denote the water stream, the inlet and the outlet of the heat exchangers, respectively. $\dot{m}$ is the mass flow rate, $c_{p,w}$ is the specific heat capacity of water and $T$ is the temperature.

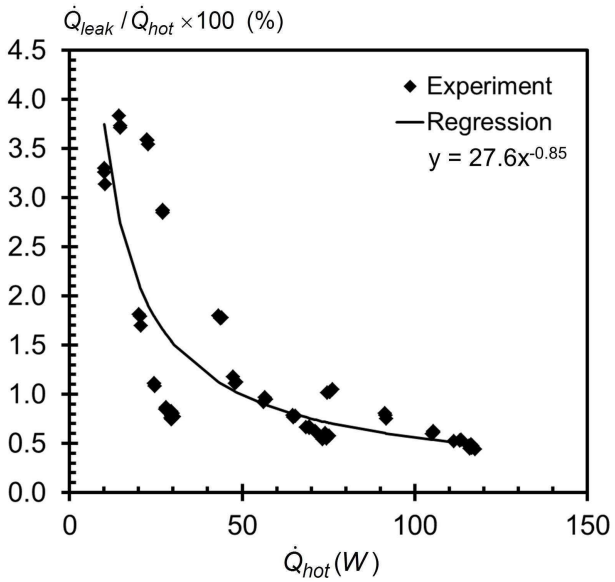


Figure 3: The relative deviation of heat leakage ($(\dot{Q}_{leak}/\dot{Q}_{hot}) \times 100\%$) as a function of heat transfer rate measured at the hot heat exchanger ($\dot{Q}_{hot}$)

The heat leakage through conduction from the heat exchangers to the surrounding was estimated using Fourier's law, based on the temperature readings recorded at various locations shown in Fig.2. This includes the heat conduction through helium gas and the resonator pipe. Fig.3 shows the relationship between the heat leakage and the heat transfer rate on the hot heat exchanger. Using a non-linear curve fitting, the function at the top-right of the plot was obtained with a coefficient of determination $R^2 = 0.86$. In the subsequent analysis, the estimated heat leakage was subtracted in advance from the heat transfer rate.

In oscillatory flow conditions, the dimensionless heat transfer coefficient, i.e. the Nusselt number ($Nu_{o,OSC}$), on the oscillatory flow side of the heat exchanger is defined as

$$Nu_{o,OSC} = \frac{h_{o,OSC} D_h}{k}. \tag{5}$$

$h_{o,OSC}$, $D_h$ and $k$ are the oscillatory flow side heat transfer coefficient, the hydraulic diameter of the channels in the heat exchangers open to the oscillatory flow and the thermal conductivity of helium at the characteristic temperature, respectively. As the heat exchangers in thermoacoustic applications are often the crossflow type of design, the gas side heat transfer coefficient ($h_{o,OSC}$) is determined using the log-mean-temperature-different (LMTD) method[17]. With the heat exchanger being treated as a fins-on-tubes configuration, the overall heat transfer coefficient of the hot heat exchanger, $UA$, is defined as follows

$$UA = \frac{\dot{Q}}{LMTD_{OSC}} = \frac{1}{\frac{1}{\eta_o h_{o,OSC} A_o} + R_{tube} + \frac{1}{h_i A_{t,i}}}. \tag{6}$$

The overall fin efficiency ($\eta_o$) is estimated to be 0.7[17]. $A_o$ and $A_{t,i}$ are the heat transfer areas on the gas side and the water side. Following the expression of the log mean temperature difference for a crossflow heat exchanger in a unidirectional flow, the log mean temperature difference in an oscillatory flow ($LMTD_{OSC}$) is defined as

$$LMTD_{OSC} = \frac{(T_{w,o} - T_{w,i})}{ln(\frac{T_b - T_{w,i}}{T_b - T_{w,o}})}. \tag{7}$$

$T_b$ is the gas temperature at section b in Fig.2. $h_i$ is the heat transfer coefficient of the heat exchangers on the water side. It was determined separately by taking measurements on the heat exchangers in unidirectional

steady flow conditions. The details of the experimental apparatus and procedure are given in[18]. The thermal resistance of the tubes ($R_{tube}$) is obtained using

$$R_{tube} = ln(r_2/r_1)/(2\pi L_T k). \tag{8}$$

where $r_2$ and $r_1$ are the outer and inner radii of the copper tubes, respectively. $L_T$ is the effective length of the tubes, through which the heat transfer to/from the gas takes place. $k$ is the thermal conductivity of the copper tubes.

In addition to presenting the thermal performance of the heat exchangers in terms of Nusselt number, an important alternative approach is the heat transfer effectiveness scheme. It was also adopted by Wakeland and Keolian[10]. Heat transfer effectiveness ($\epsilon$) is a dimensionless parameter defined as the ratio of the actual heat transfer rate ($\dot{Q}_{exp}$) of a heat exchanger to the maximum possible heat transfer rate ($\dot{Q}_{max}$) in the form of

$$\epsilon = \dot{Q}_{exp}/\dot{Q}_{max}. \tag{9}$$

The actual heat transfer rate ($\dot{Q}_{exp}$) is obtained from measurements using Eq.(4). The maximum possible heat transfer rate ($\dot{Q}_{max}$) represent the heat transfer rate achievable between the heat source and the sink, which is given by

$$\dot{Q}_{max} = \dot{m}_{osc} c_p (T_h - T_c). \tag{10}$$

$c_p$ is the isobaric specific heat capacity of the gas. $T_h$ and $T_c$ are the temperatures of hot and cold heat exchangers, respectively. The mean values of the temperatures at the inlet and outlet of the heat exchangers were applied. $\dot{m}_{osc}$ is the mass flow rate of the gas that oscillates between the hot and cold heat exchangers, which can be calculated using

$$\dot{m}_{osc} = \rho_m A_c x_{eff} f. \tag{11}$$

$\rho_m$, $A_c$, $x_{eff}$ and $f$ are the mean density of gas, the open area of the heat exchanger to the gas flow, the effective length and the oscillating frequency, respectively. The effective length $x_{eff}$ is defined as:

$$x_{eff} = \begin{cases} 2\xi_a & \text{for} \quad 2\xi_a < L \\ L & \text{for} \quad 2\xi_a \geq L. \end{cases} \tag{12}$$

From the definition of the hydraulic radius, the open area ($A_c$) relates to the hydraulic radius ($r_h = D_h/4$) and the fin wetted perimeter ($\Pi$) by

$$A_c = r_h \Pi. \tag{13}$$

Using the thermal penetration depth in Eq.(1) and the open area in Eq.(13), the maximum possible heat transfer rate ($\dot{Q}_{max}$) in Eq.(10) can be re-arranged as

$$\dot{Q}_{max} = [(T_h - T_c) k \Pi] x_{eff} \frac{r_h}{\pi {\delta_\kappa}^2}. \tag{14}$$

The experimental results of heat transfer effectiveness ($\epsilon$) from Eq.(9) are then correlated to the dimensionless parameters $(\xi_a - g)/(\sigma L)$ and $D/\delta_\kappa$ in order to obtain a correlation for the estimation of the heat transfer rate in oscillatory flow conditions.

## 5. Measurement uncertainty

The overall measurement uncertainty in the experimental results consists of several components that can be categorized into two groups, the precision or random error, and the systematic or fixed error, depending on the estimation method used[19, 20].

The majority of uncertainty considered in this study arose from the measurement of the mass flow rates and the temperatures of water. In addition, as seen in Eq.(6), the uncertainty in the estimation of $h_i$ , which is mainly the regression uncertainty, will also propagate to the heat transfer results. The regression uncertainty is obtained from the standard deviation of the estimated results from the $h_i$ correlation[21].

The uncertainty of the heat transfer coefficient ($U_{h_{o,OSC}}$) can be found according to the error propagation equation as follows[22]

$$U_{h_{o,OSC}}{}^2 = \sum_i (\frac{\partial h_{o,OSC}}{\partial x_i})^2 (P_{x_i}{}^2 + B_{x_i}{}^2). \tag{15}$$

Here $x_i$ is any of the parameters in Eq.(6), $P_{x_i}$ and $B_{x_i}$ are the precision and systematic errors of the parameter $x_i$. Similarly, the uncertainty ($U_{Nu_{o,OSC}}$) of the non-dimensional heat transfer coefficient from experiments ($Nu_{o,OSC}$) is obtained as:

$$U_{Nu_{o,OSC}}{}^2 = \sum_i (\frac{\partial Nu_{o,OSC}}{\partial y_i})^2 (P_{y_i}{}^2 + B_{y_i}{}^2). \tag{16}$$

$y_i$ is any of the parameters in Eq.(5). In this experimental study, the overall uncertainty of Nusselt number ranges from 7 - 23%, evaluated at 95% confidence level. The uncertainty tends to be higher for a low heat transfer rate when the temperature difference may have been as low as 1.0 °C.

## 6. Results and discussion

The data from measurements are used to find Nusselt number and the heat transfer effectiveness at the corresponding conditions. In this section, the dependence of Nusselt number ($Nu_{o,OSC}$) on parameters such as $(\xi_a - g)/(\sigma L)$ and $D/\delta_\kappa$ will be discussed. The relationship found in this work between Nusselt number and the flow condition in terms of acoustic Reynolds number is then compared with some models and empirical correlations. A new correlation based on heat transfer effectiveness for the estimation of the heat transfer rate in oscillatory flow is also proposed.

### *6.1. Effect of $(\xi_a - g)/(\sigma L)$ on Nusselt number ($Nu_{o,OSC}$)*

The gas side heat transfer coefficient in oscillatory flow ($h_{o,OSC}$) is evaluated using Eq.(6). The obtained $h_{o,OSC}$ is then cast into a Nusselt number ($Nu_{o,OSC}$) following Eq.(5). The variation of $Nu_{o,OSC}$ with $(\xi_a - g)/(\sigma L)$ for various $D/\delta_\kappa$ ratios are shown in Fig.4. It is examined for three hot heat exchangers, all at the inlet temperature ($T_{h,i}$) of 80 °C. Lines connecting symbols are for visual guidance only.

For heat exchanger 'A' (0.7 mm HEX) (Fig.4a), it can be seen that $Nu_{o,OSC}$ increases quickly when the normalized gas displacement amplitude $(\xi_a - g)/(\sigma L)$ changes from -0.04 to around 0.5 when the gas peak-to-peak displacement amplitude is equivalent to the fin length. This change of $Nu_{o,OSC}$ is expected and considered to be caused by the increase of the effective heat exchange area. When $0 < (\xi_a - g)/(\sigma L) < 0.5$, some gas parcels are in contact with only one heat exchanger during the whole oscillation cycle. The heat transported, if there were any, by this group of gas parcels from one place to another on the same heat exchanger results in no effective heat transferred between the heat exchangers. Of the gas in contact with either of the heat exchangers, only a part is able to reach the adjacent heat exchanger and contributes to the effective heat transfer. When the displacement amplitude increases, a larger part of gas can take part in the heat transportation between the two heat exchangers, which leads to a higher Nusselt number.

Contrary to our expectation of a peak in $Nu_{o,OSC}$ around $(\xi_a - g)/(\sigma L)$ at 0.5 when the gas peak-to-peak displacement amplitude equals to the fin length, $Nu_{o,OSC}$ continues to increase at a lower rate for $(\xi_a - g)/(\sigma L) > 0.5$. This behaviour could be connected with the increased velocity at a higher displacement. Although the thermal penetration depth in Eq.1 is constant when the oscillation frequency is fixed, the temperature gradient in the thermal boundary layer could be increased due to the increasing velocity, which will enhance the heat transfer. This speculation, however, has yet to be verified. Similar effect of $(\xi_a - g)/(\sigma L)$ on $Nu_{o,OSC}$ can be observed for heat exchanger 'B' (1.4 mm HEX) and 'C' (2.1 mm HEX) as shown in Fig.4b and 4c, respectively.

In contrast to varying the gas displacement amplitude while keeping the heat exchanger length constant in this study, Besnoin and Knio[4] in their numerical investigation changed the length of the fin-type heat exchanger independently and maintained the gas displacement amplitude. The length of the cold heat exchanger examined was between 0.35 and 5.65 mm, relatively small compared to the gas displacement

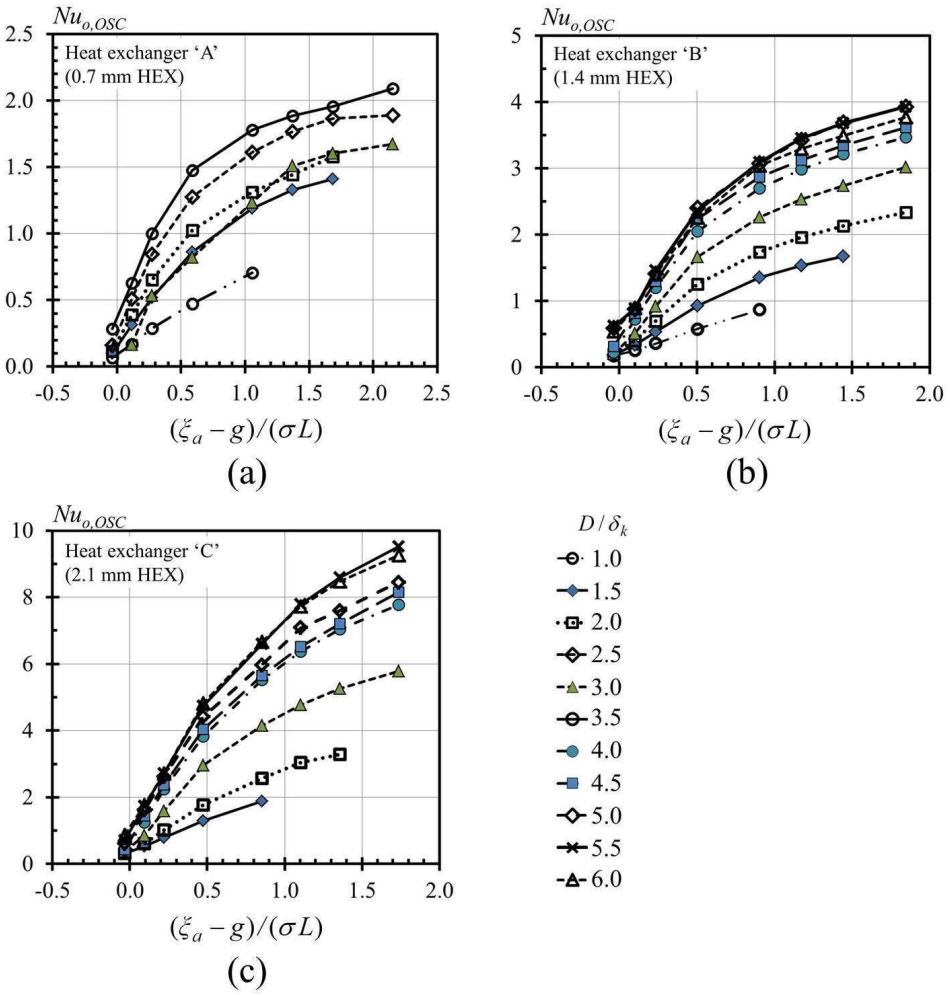


Figure 4: Dependence of $Nu_{o,OSC}$ on $(\xi_a - g)/(\sigma L)$ at various $D/\delta_\kappa$ for $T_{h,i}$ at 80 °C

amplitude. As a result, $(\xi_a - g)/L$ was varied from 1.1 to 5.1. It was shown that, when $(\xi_a - g)/L$ increases, the total heat flux, hence the heat transfer coefficient, increases before it reaches a maximum value and decreases. A local reverse heat flux could be observed at the edge of the plates, which was also observed by Piccolo and Pistone[8]. The result shows that there is an optimal heat exchanger length to keep the reverse heat flux minimum and to maximize the total heat flux for a given gas displacement amplitude. The optimal heat exchanger length ($L_{opt}$) was found in between 0.05 - 0.25 times ($2\xi_a + \delta_\kappa$), based on the assumptions made for the numerical scheme. This is somewhat smaller than what has been suggested[3, 16].

Also in their result[4], Besnoin and Knio showed that for the same heat exchanger length and gap width, the total heat flux from heat exchangers (and accordingly the heat transfer coefficient) increased when the gas displacement amplitude was higher (cf. cases 8 - 10 and 32 - 34 in [4]). This general trend is in agreement with our observations. It was shown that the optimal heat exchanger length was slightly smaller for a higher gas displacement amplitude. This implies that if a heat exchanger is designed with an optimal length for a low displacement amplitude, it can still be used at a higher displacement amplitude and would still have a high heat transfer coefficient overall.

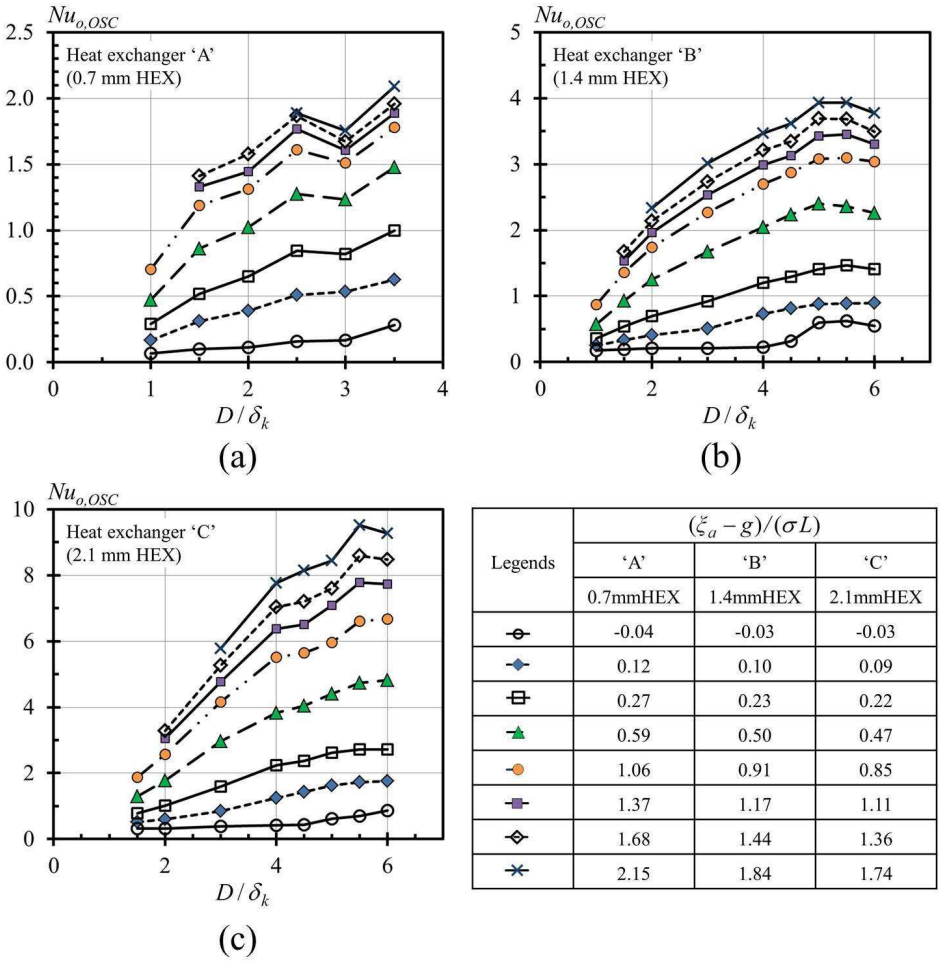


| Legends | $(\xi_a - g)/(\sigma L)$ | | |
|---|---|---|---|
| | 'A' | 'B' | 'C' |
| | 0.7mmHEX | 1.4mmHEX | 2.1mmHEX |
| | -0.04 | -0.03 | -0.03 |
| | 0.12 | 0.10 | 0.09 |
| | 0.27 | 0.23 | 0.22 |
| | 0.59 | 0.50 | 0.47 |
| | 1.06 | 0.91 | 0.85 |
| | 1.37 | 1.17 | 1.11 |
| | 1.68 | 1.44 | 1.36 |
| | 2.15 | 1.84 | 1.74 |

Figure 5: Dependence of $Nu_{o,OSC}$ on $D/\delta_\kappa$ at various $(\xi_a - g)/(\sigma L)$ for $T_{h,i}$ at 80 °C

*6.2. Effect of $D/\delta_\kappa$ on Nusselt number ($Nu_{o,OSC}$)*

The relation between $Nu_{o,OSC}$ and the normalized fin spacing $D/\delta_\kappa$ for the three heat exchangers is shown in Fig. 5, when the hot water inlet temperature ($T_{h,i}$) is 80 °C . The lines are added for visual guidance. Consider heat exchanger 'B' (Fig. 5b) that was tested on the full range of $D/\delta_\kappa$. For all $(\xi_a - g)/(\sigma L)$ investigated, the values of $Nu_{o,OSC}$ steadily increase with $D/\delta_\kappa$ until they reach maximum values around $D/\delta_\kappa = 5.0$. The decrease of $Nu_{o,OSC}$ values occurs when $D/\delta_\kappa$ increases further.

The increase in $Nu_{o,OSC}$ when $D/\delta_\kappa$ changes from 1.0 to 5.0 agrees with the observation made by Besnoin and Knio (cf. Fig. 15 of [4]), where both the mean heat flux and the power density, and consequently the heat transfer coefficient, increase with the fin spacing. It is considered to be partly caused by the variation of the effective *heat exchange length*. It is known that a net heat transfer between the oscillatory flow and its adjacent plate-form stacks or fin type heat exchangers takes place only at the plate edge[4, 5, 8, 15]. It is within this heat exchange length that there is a non-zero time averaged heat flux from/to the plates. Piccolo and Pistone[8] reported that for a given oscillation amplitude of the flow, the *heat exchange length* rapidly increases with $D/\delta_\kappa$ when $D/\delta_\kappa < 2.0$. The heat exchange length continues to increase till $D/\delta_\kappa$ is around 5.0, after which there is little change in the heat exchange length.

For $D/\delta_\kappa > 5.0$, the decrease in $Nu_{o,OSC}$ can be clearly observed for most of the values of $(\xi_a - g)/(\sigma L)$ investigated (Fig. 5b). Besnoin and Knio[4] has a very similar observation on a short heat exchanger. In

Table 2: Regression results for the steady flow experiment

| Nusselt number | Heat exchanger | | |
|---|---|---|---|
| | A | B | C |
| Steady flow ($Nu_{o,STD}$) | $0.13Pr^{1/3}{Re_0}^{0.71}$ | $0.21Pr^{1/3}{Re_0}^{0.70}$ | $1.76Pr^{1/3}{Re_0}^{0.34}$ |
| Oscillatory flow ($Nu_{o,RMS-Re}$) | $0.10Pr^{1/3}{Re_1}^{0.71}$ | $0.16Pr^{1/3}{Re_1}^{0.70}$ | $1.56Pr^{1/3}{Re_1}^{0.34}$ |

their study $\delta_\kappa$ was kept constant while the fin spacing $D$ was varied. Maximum values of the power density at two acoustic excitation levels can be clearly identified, both when $D/\delta_\kappa$ is at 3.5. The mean heat flux, however, peaks when $D/\delta_\kappa$ is around 10. The cause is likely to be related to the fin spacing, the *heat exchange length*, and the underlying gas flow and heat transfer mechanism. In this work, a fixed fin spacing would mean that both the mean heat flux and the power density show the same trend and peak at the same $D/\delta_\kappa$. However, it remains puzzling what causes the decline of the heat transfer coefficient when $D/\delta_\kappa$ is high and futher study into the more detailed flow and temperature fields may be required.

In Fig. 5a, no peak of $Nu_{o,OSC}$ for heat exchanger 'A' (0.7 mm HEX) can be identified before $D/\delta_\kappa$ reaches the maximum value of 3.5 due to the limit in the system pressure. The results for heat exchanger 'C' (2.1 mm HEX) are presented in Fig. 5c. The change of $Nu_{o,OSC}$ with $D/\delta_\kappa$ can be seen very similar to that for heat exchanger 'B'. However, the $Nu_{o,OSC}$ peaks when $D/\delta_\kappa = 5.5$.

For the cases when the water temperatures at the inlet of the hot heat exchanger ($T_{h,i}$) are 60 and 40 °C, respectively, the results (not shown) exhibit a similar trend to that observed when $T_{h,i}$ is 80 °C (Fig. 5). The Nusselt number grows with the increasing $D/\delta_\kappa$ and tends to decrease after a particular $D/\delta_\kappa$ value. Overall, the values of the Nusselt number reach maximum when $D/\delta_\kappa$ is between 5.0 and 5.5.

### *6.3. Comparison with other heat transfer models*

In this section, the experimental results are compared with other physical models, such as the RMS-Re model, the TASFE model[23], the boundary layer conduction model[24, 25], the model integrating the Valensi number (Va)[13, 26], and some of their variations.

#### *6.3.1. Root Mean Square Reynolds Number (RMS-Re) models*

The RMS-Re model is based on the heat transfer correlation for a heat exchanger in a steady flow. With the consideration that the acoustically induced flow normally has a sinusoidal velocity, the RMS-Re model is obtained by substituting the Reynolds number in the gas side heat transfer correlation with the rms acoustic Reynolds number. In this work, the heat transfer correlations in a steady flow for the heat exchangers of interest were obtained from the regression of experimental data[18] and are given in Table 2. The rms acoustic Reynolds number is defined as:

$$Re_{rms} = \rho_m D_h u_{rms}/\mu. \tag{17}$$

Here, $\mu$ is the dynamic viscosity of gas at the mean temperature. For a simple sinusoidal acoustic wave, the rms acoustic velocity, $u_{rms}$, is $u_1/\sqrt{2}$. The acoustic Reynolds number ($Re_1$) is defined as $\rho_m D_h u_1/\mu$, hence $Re_{rms} = Re_1/\sqrt{2}$. After the substitution, the heat transfer correlations in oscillatory flow conditions in terms of ($Nu_{o,RMS-Re}$) are obtained and shown in Table 2.

Based on the data regression of their experimental results on a finned-tube heat exchanger, Nsofor et al.[12] proposed a correlation, which is given as follows for later comparison

$$Nu = 0.61Pr^{0.11}{Re_{rms}}^{0.31} = 0.548Pr^{0.11}{Re_1}^{0.31}. \tag{18}$$

#### *6.3.2. Time-Average Steady-Flow Equivalent (TASFE) models*

Another physical model is the TASFE model. It is derived based on the assumption that the heat transfer between a heat exchanger and an oscillatory flow with zero mean flow is equivalent to the time-average over an oscillation cycle of the heat transfer under steady flow condition. The heat transfer correlations for the

Table 3: Absolute deviation (%) of heat transfer rates estimated using different models and correlations

| Models and correlations | Heat exchanger | | | |
|---|---|---|---|---|
| | 'A' | 'B' | 'C' | Average |
| | $D/\delta_\kappa$=3.5 | $D/\delta_\kappa$=6.0 | $D/\delta_\kappa$=6.0 | |
| RMS-Re | 53.0 | 71.3 | 51.8 | 58.7 |
| TASFE | 48.4 | 65.1 | 43.7 | 52.4 |
| Boundary layer conduction | 50.3 | 52.1 | 21.8 | 41.4 |
| Paek et al.[11] | 26.3 | 38.0 | 29.4 | 31.2 |
| Nsofor et al.[12] | 45.2 | 28.3 | 16.7 | 30.0 |
| Zhao and Cheng[26] | 19.6 | 23.8 | 46.3 | 29.9 |
| Tang et al.[13] | 39.9 | 34.9 | 13.3 | 29.4 |
| Garrett et al.[27] | 34.0 | 30.6 | 15.8 | 26.8 |
| Heat transfer effectiveness ($\epsilon$) | 5.1 | 4.5 | 6.7 | 5.4 |

interested heat exchangers in a steady flow has been given in Table 2. In a simple sinusoidal acoustic wave, the instantaneous velocity reads $u_1 \sin \omega t$, and the instantaneous acoustic Reynolds number can be written as $(\rho D_h u_1 \sin \omega t)/\mu$ or $Re_1 \sin \omega t$. Let $e$ and $n$ be the constants in the heat transfer correlations for each of the heat exchangers in steady flow given in Table 2. Replace the steady flow Reynolds number ($Re_{o,STD}$) with the instantaneous acoustic Reynolds number, and take the time average over an oscillation cycle. The heat transfer correlations in the TASFE model can be written as:

$$\begin{aligned} Nu_{o,TASFE} &= \frac{\omega}{\pi} \sum_{0}^{\pi/\omega} ePr^{1/3} (Re_1 \sin \omega t)^n dt \\ &= ePr^{1/3} {Re_1}^n \frac{\omega}{\pi} \sum_{0}^{\pi/\omega} (\sin \omega t)^n dt \end{aligned} \tag{19}$$

Paek et al.[11] proposed a modified TASFE model by introducing a correction factor, in order to take into account the fact that the gas temperature is not the same for each half of an oscillation cycle. The correction factor of 0.353 was obtained from a regression analysis. By multiplying the acoustic Reynolds number in Eq. (19) by the conversion factor, the modified TASFE model was shown to predict the heat transfer correlation better than the original TASFE model[11].

Figure 6a shows the values of $Nu_{o,OSC}$ obtained from various models for heat exchanger 'A' (0.7 mm HEX) when $D/\delta_\kappa = 3.5$, while Figs. 6b and 6c represent heat exchangers 'B' (1.4 mm HEX) and 'C' (2.1 mm HEX), respectively, when $D/\delta_\kappa = 6.0$. The results for $T_{h,i} = 80\,^\circ$C are presented.

For the RMS-Re and TASFE models, a continuous increase of the predicted heat transfer coefficient with the increase of the acoustic Reynolds number ($Re_1$) can be observed for all tested conditions. For any given condition, the value of $Nu_{o,RMS-Re}$ is always higher than that of $Nu_{o,TASFE}$. This is due to the fact that the Reynolds number obtained from the RMS-Re model is larger than that from the TASFE model. The values of $Nu_{o,RMS-Re}$ and $Nu_{o,TASFE}$ are much higher than the experimental results at all conditions. Similar to the original TASFE model, the modified TASFE model proposed by Paek et al.[11] overestimates the Nusselt number. This may indicate that the modified TASFE model with a correction factor of 0.353 is not applicable to heat exchangers with different geometries and operating conditions. The differences between the heat transfer rates from various models and empirical correlations and the measured heat transfer rates for heat exchangers 'A', 'B' and 'C' respectively and on average, in terms of absolute deviations, are summarized in Table 3. The data correspond to selected conditions as examples, that is, $D/\delta_\kappa$ is 3.5 for heat exchanger 'A', 6.0 for heat exchanger 'B' and 6.0 for heat exchanger 'C', respectively.

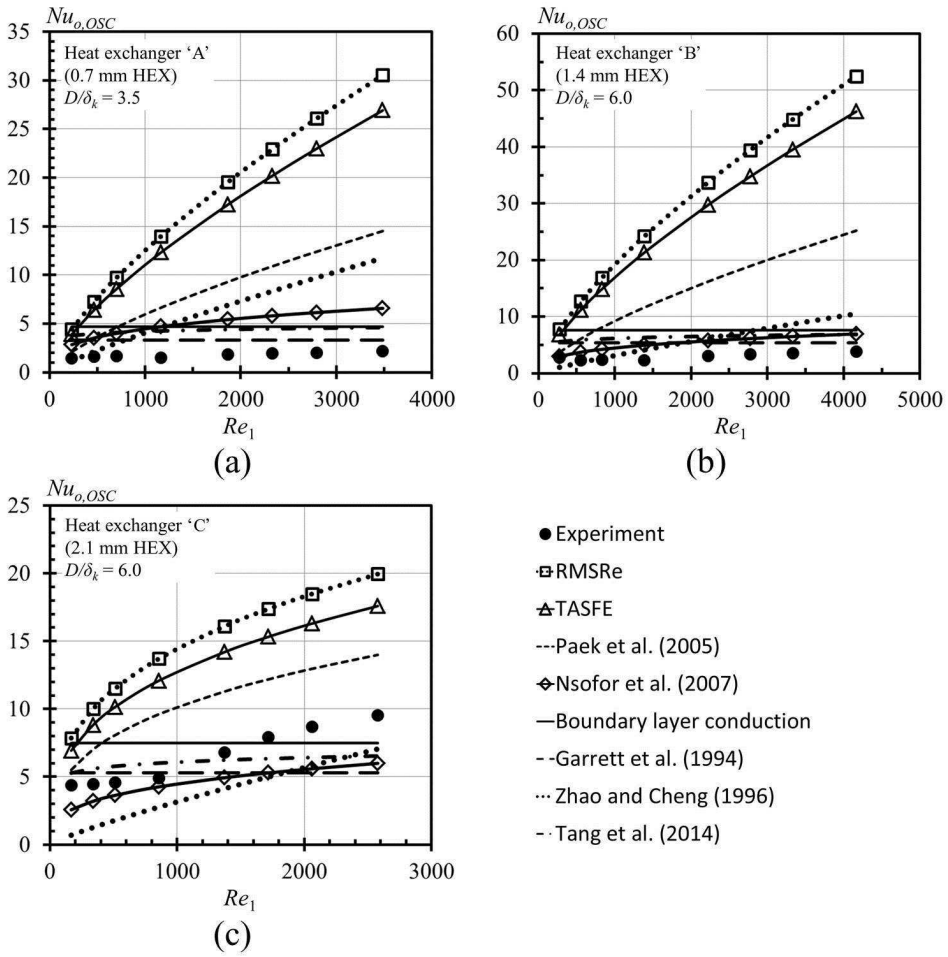


Figure 6: Nusselt number ($Nu_{o,OSC}$) versus acoustic Reynolds number ($Re_1$) at $T_{h,i} = 80\,^{\circ}\mathrm{C}$

*6.3.3. Boundary layer conduction model*

A third model for the evaluation of heat transfer from heat exchangers in oscillating flow ($h_{o,OSC}$) was suggested by Swift[24] and Ward et al.[25]. The convective heat transfer coefficient on the gas side of the heat exchanger is simply taken as the ratio of the fluid thermal conductivity to the smaller one of the hydraulic radius and the thermal penetration depth, which is defined as follows:

$$h_{o,OSC} = \frac{k}{min(r_h, \delta_\kappa)}. \tag{20}$$

The estimated $h_{o,OSC}$ is used to calculate $Nu_{o,OSC}$ using Eq. (5). It can be seen in Fig. 6 that the boundary layer conduction model on every condition yields a constant Nusselt number value, reflecting the independence of the heat transfer coefficient ($h_{o,OSC}$) and Nusselt number ($Nu_{o,OSC}$) from the acoustic Reynolds number ($Re_1$) and the gas displacement amplitude ($\xi_a$).

Garrett et al.[27] modified the original model to examine the heat transfer coefficient ($h_{o,OSC}$) and Nusselt number ($Nu_{o,OSC}$) of their finned-tube heat exchanger in oscillatory flows. Garrett et al.[27] suggested that the heat transfer rate in oscillating flows was a time-dependent sinusoidal function. Thus, the heat transfer coefficient can be better represented by the root-means-square value ($h_{o,OSC/rms}$) as follows

$$h_{o,OSC/rms} = \frac{h_{o,OSC}}{\sqrt{2}}, \tag{21}$$

where $h_{o,OSC}$ is obtained from the original boundary layer conduction model using Eq. (20). The calculated Nusselt number obtained by this modified model is presented by a long dash line in Fig. 6. Generally speaking, the prediction using this approach has a better agreement with the experimental result than the original model proposed by Swift [24] and Ward et al.[25]. However, overestimations for the heat exchanger 'A' (0.7 mm HEX) and 'B' (1.4 mm HEX) can be observed, whereas predictions for heat exchanger 'C' (2.1 mm HEX) are sometimes underestimated.

*6.3.4. The Valensi number integrated heat transfer model*

Correlations combining the Valensi number ($Va$) and the acoustic Reynolds number ($Re_1$) to estimate the Nusselt number in oscillatory flow ($Nu_{o,OSC}$) were proposed by Zhao and Cheng [26] and Tang et al.[13]. The Valensi number represents the ratio of the hydraulic diameter for the channels between heat transfer fins to the distance of momentum diffusion during one oscillating cycle, which is expressed by

$$Va = \frac{\rho\omega {D_h}^2}{\mu}. \tag{22}$$

Zhao and Cheng[26] carried out an experiment on a laminar reciprocating flow of air in a long tube with constant heat flux. They proposed a model integrating the Valensi number into the correlation of the Nusselt number, which reads as follow

$$Nu_{o,OSC/Z} = 0.02 {A_Z}^{0.85} {Re_\omega}^{0.58}. \tag{23}$$

Parameters $Re_\omega$ and $A_Z$ are defined as

$$Re_\omega = \frac{\rho\omega {D_i}^2}{\mu} = Va, \tag{24}$$

and

$$A_Z = \frac{\xi_a}{D_i} = 2\frac{Re_1}{Va}. \tag{25}$$

$D_i$ is the internal tube diameter. The operating conditions were in the range of $23 < Re_\omega < 464$ and $8.5 < A_Z < 34.9$ in their experimental study.

Substituting Eq. (24) and (25) into (23), the correlation above can be rewritten as:

$$Nu_{o,OSC/Z} = 0.036{Re_1}^{0.85}Va^{-0.27}. \quad (26)$$

Tang et al.[13] also proposed a correlation in the format of Eq. (26) as follows

$$Nu_{o,OSC/T} = 0.469{Re_1}^{0.0747}Va^{0.395}. \quad (27)$$

The correlation above was obtained from a circular shape fin-type heat exchanger with cooling water flowing in a channel formed around the circumference of the heat exchanger. The fin is 0.75 mm thick, with a fin spacing of 0.75 mm, while the fin length measured in the flow direction is 20 mm. The flow conditions investigated were in the range of $150 < Va < 350$, whereas in this study the Valensi number is in the range of $5 < Va < 184$.

The comparison shows that the correlation proposed by Tang et al.[13] gives a higher Nusselt number at low acoustic Reynolds numbers and a lower Nusselt number at high acoustic Reynolds numbers than that by Zhao and Cheng[26]. When compared with the experimental results, the predictions from these correlations are generally larger than the experimental results for heat exchanger 'A' (0.7 mm HEX). There is a better agreement between the correlations and the experimental results for heat exchanger 'B' (1.4 mm HEX). For heat exchanger 'C' (2.1 mm HEX), the correlations underestimate the Nusselt number.

There is clearly difference between the values of the Nusselt number obtained using the correlations by Zhao and Cheng[26] and Tang et al.[13] and the experimental results in the current study (cf. Table 3). The causes of this discrepancy could be directly related to the heat exchanger configurations, the working medium and the operating conditions among others. In the study by Zhao and Cheng[26], the experiment was performed in a long copper tube with constant heat flux, and air was used as working fluid. The gas properties, for instance Prandtl number ($Pr$), are not included in the correlations. A fin-type heat exchanger was used by Tang et al.[13], compared to the finned-tubes heat exchanger used in this study. The heat transfer in internal oscillatory flows and external oscillatory flows over plates of finite length and cylinders will be different to some extent. A more appropriate like-for-like comparison of the heat transfer correlations for heat exchangers of various design is hindered by the lack of experimental and numerical studies in this area.

### *6.4. Heat transfer effectiveness* ($\epsilon$)

An alternative approach to correlate the thermal performance of a heat exchanger with the flow conditions based on heat transfer effectiveness ($\epsilon$) is described in this section. This model incorporates the heat transfer capacity, which is the ability to transfer heat at a given temperature difference. Figures 7(a) and (b) show the heat transfer rate as a function of $D/\delta_\kappa$, for heat exchanger 'B' (1.4 mm HEX) when $(\xi_a - g)/(\sigma L) = 0.5$.

The heat transfer rates ($\dot{Q}_{exp}$) from measurements and the maximum possible heat transfer rate ($\dot{Q}_{max}$) at different inlet temperatures ($T_{h,i}$) of water are plotted in the same graph. Figure 7(a) presents the results on a linear scale, and Fig. 7(b) on a log-log scale. The experimental data were collected from three cases when the values of the inlet temperature ($T_{h,i}$) of water were at 40, 60, and 80 °C, respectively.

The ratio of $\dot{Q}_{exp}$ to $\dot{Q}_{max}$ yields the heat transfer effectiveness ($\epsilon$), as shown in Fig. 7(c). The curves of the heat transfer effectiveness for all inlet temperatures ($T_{h,i}$) collapse into one single line. This implies that the heat transfer effectiveness of a heat exchanger is independent of its operating temperature. This is further confirmed by that, the relative difference between the heat transfer effectiveness ($\epsilon$) evaluated at any inlet temperature of water ($T_{h,i}$) and the average value of all heat transfer effectiveness values from all inlet temperatures of water at any given $(\xi_a - g)/(\sigma L)$ and $D/\delta_\kappa$ is not more than 2.8%. Thus, the measurement data for different $T_{h,i}$ but at the same $(\xi_a - g)/(\sigma L)$ and $D/\delta_\kappa$ are combined for subsequent analysis.

The results of heat transfer effectiveness ($\epsilon$) from all heat exchangers at all operating conditions are shown in Fig. 8. In the same figure, experimental data from [10] are plotted with $(\xi_a - g)/(\sigma L)$ at 1.0, 1.9 and 2.8 as examples. It can be seen that the results from the current study are clustered in three groups, which corresponds to the three heat exchangers of different fin spacings. Generally speaking, at the same $D/\delta_\kappa$, the values of heat transfer effectiveness for heat exchanger 'C' (2.1 mm HEX) are higher than those for heat exchangers 'B' (1.4 mm HEX) and 'A' (0.7 mm HEX).

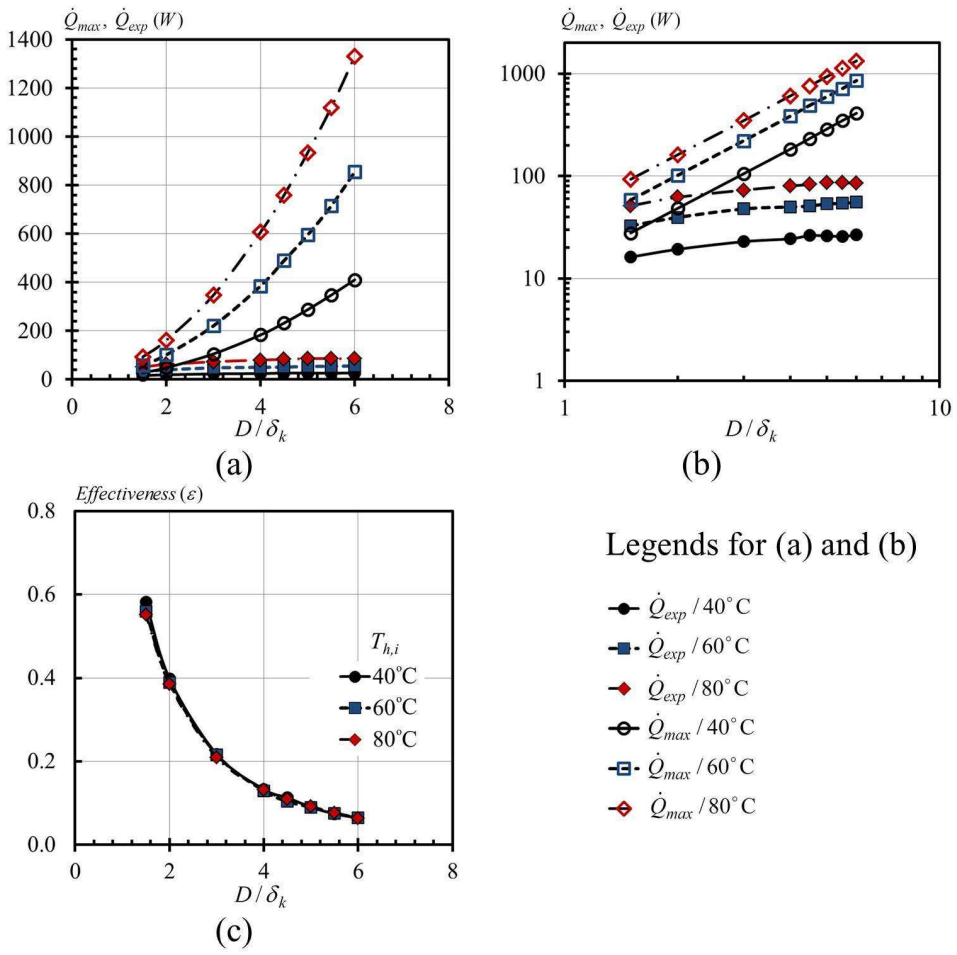


Figure 7: Heat transfer rate on a linear scale (a), on a log-log scale (b), and the heat transfer effectiveness ($\epsilon$) versus $D/\delta_\kappa$ (c). All data are for heat exchanger 'B' (1.4 mm HEX) with $(\xi_a - g)/(\sigma L) = 0.5$.

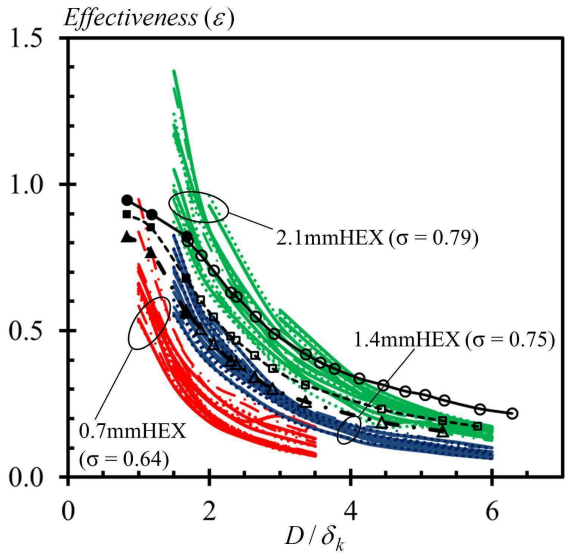


Figure 8: Heat transfer effectiveness ($\epsilon$) from current work (lines) and experiments by Wakeland and Keolian[10] (symbols with connecting lines).

A suspicious occurrence of high heat transfer effectiveness can be noticed when $D/\delta_\kappa$ goes below 2.0. The heat transfer effectiveness exceeds 1.0, more specifically for heat exchanger 'C' (2.1 mm HEX). By definition, a value of the heat transfer effectiveness above unity means that the actual heat transfer rate is greater than the maximum available heat transfer rate calculated using Eq. (10).

Unlike the experimental results obtained in this study, the heat transfer effectiveness ($\epsilon$) obtained by Wakeland and Keolian[10] seem to approach unity when the ratio $D/\delta_\kappa$ decreases to 1.0. It is worth noting that in their experiments, two different heat exchanger configurations were used. The data for $D/\delta_\kappa > 1.7$ was obtained when there was a 'small gap' of 5.5 mm in between two heat exchangers, and the results for $D/\delta_\kappa < 1.7$ was obtained using the same pair of heat exchangers, but with a 'large gap' of 16.3 mm in between. However, the dependence of the heat transfer performance on the gap between heat exchangers remains unclear.

In the evaluation of the heat transfer effectiveness, the maximum possible heat transfer rate ($\dot{Q}_{max}$) represents the quantity of heat that can be transported between two heat reservoirs at the given temperatures by the working gas in certain flow rate ($\dot{m}_{OSC}$). The mass flow rate $\dot{m}_{OSC}$ is obtained by incorporating parameters such as $x_{eff}$ and $f$ for an oscillatory flow (cf. Eq. (11)).

$\dot{m}_{OSC}$ is equivalent to the mass flow rate of gas having a mean density of $\rho_m$, moving in a unidirectional steady flow through a cross-sectional area of $A_c$, to a distance of $x_{eff}$ from its initial location during a time period of $1/f$. In this definition of $\dot{m}_{OSC}$, the analogy to steady flow conditions may not truly reflect the characteristics of oscillatory flow, such as the development of velocity and thermal boundary layer that are particularly important to heat transfer process. It is hence possible that the heat transfer effectiveness ($\epsilon$) is higher than one when the actual heat transfer is enhanced in oscillatory flow.

As illustrated in Fig. 8, the variation of the heat transfer effectiveness in relation to $D/\delta_\kappa$ falls into three clusters closely related to the fin spacings of the heat exchangers. Hence, heat transfer effectiveness correlation is determined for each heat exchanger separately. The change of the heat transfer effectiveness in relation to $D/\delta_\kappa$ agrees well with an exponential function. Data regression was carried out using the non-linear curve fitting function based on the Simplex algorithm (also known as Nelder-Mead) in order to find the parameters $b$ and $c$ in the equation as follows

$$\epsilon = exp(-5.64 + \frac{b}{D/\delta_\kappa + c}). \tag{28}$$

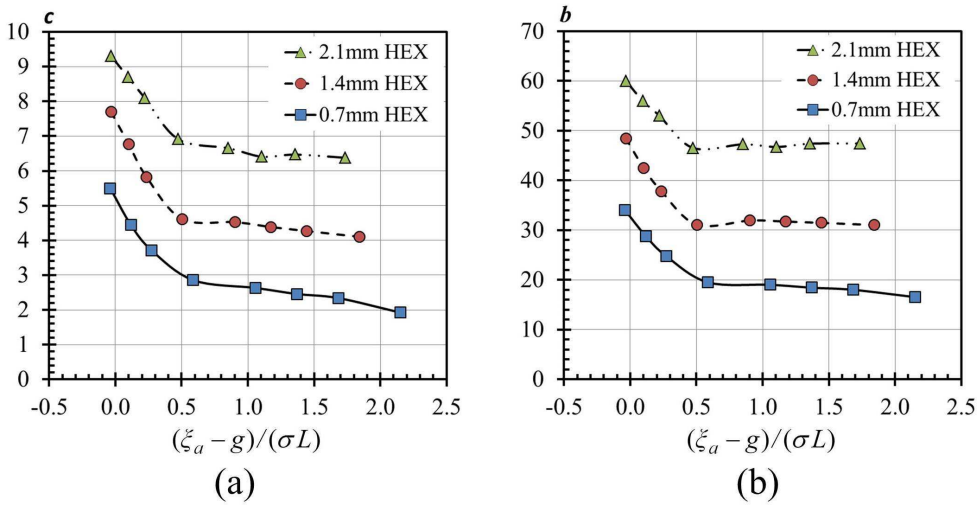


Figure 9: Parameters $b$ and $c$ in Eq. (28) as a function of $(\xi_a - g)/(\sigma L)$.

The parameters $b$ and $c$ are functions of $(\xi_a - g)/(\sigma L)$, which are plotted in Fig. 9.

The heat transfer rate can be estimated using Eq. (9), once the heat transfer effectiveness is determined using Eq. (28). Fig. 10 shows the estimated heat transfer rate from the heat transfer effectiveness correlation ($\dot{Q}_{est}$) together with the measured heat transfer rate ($\dot{Q}_{exp}$). A good agreement can be observed. The experimental results shown in Fig. 10 were taken when the inlet temperature of water ($T_{h,i}$) was at 80 °C. Similar comparison (not shown) when the inlet temperature of water, $T_{h,i}, wasat40$ and 60 °C respectively, show very similar trend in general. The difference between the estimated heat transfer rate and the heat transfer rate from experiments is illustrated in Fig. 11 for three heat exchangers at all tested conditions.

In Fig. 12, the heat transfer rates from measurements for selected conditions are compared with the estimated values from various models and empirical correlations previously discussed. As can be seen, the heat transfer rate for heat exchanger 'A' (0.7 mm HEX) and 'B' (1.4 mm HEX) are almost always overestimated. For the heat exchanger 'C' (2.1 mm HEX), some empirical correlations underestimate the heat transfer rate, especially at high Reynolds numbers. The difference between the estimated values and the experimental results, in terms of absolute deviation, is summarized in Table 3. Generally, the estimations from models, such as the RMS-Re, the TASFE and the boundary layer conduction models, show high deviation values for individual heat exchangers and on average. Other empirical correlations, which were mainly developed for specific heat exchangers on certain range of operating conditions, surprisingly have smaller deviations overall from the experimental results in this work. In particular, the correlations developed by Zhao and Cheng[26] and Paek et al.[11] have smaller deviations on the heat exchangers 'A' (0.7 mm HEX), than those on heat exchangers 'B' (1.4 mm HEX) and 'C' (2.1 mm HEX). The boundary layer conduction model and the correlations proposed by Tang et al.[13], Nsofor et al.[12] and Garrett et al.[27] demonstrate smaller deviation on heat exchanger 'C' (2.1 mm HEX). It can also be seen that the developed correlation of the heat transfer effectiveness ($\epsilon$) can predict the heat transfer rate for all three tested heat exchangers to a fairly good accuracy, with an average deviation of 5.4%.

## 7. Conclusions

An experimental apparatus for the study of heat transfer from some finned-tube heat exchangers in oscillatory flows has been developed. Heat transfer performance was experimentally investigated on three heat exchanger at various testing conditions. The influence of normalized fin length ($(\xi_a - g)/(\sigma L)$) and normalized fin spacing ($D/\delta_\kappa$) on Nusselt number ($Nu_{o,OSC}$) was under examination. For heat exchanger 'A' with the narrowest fin spacing, the values of $Nu_{o,OSC}$ increase very rapidly for $(\xi_a - g)/(\sigma L) < 0.5$. The

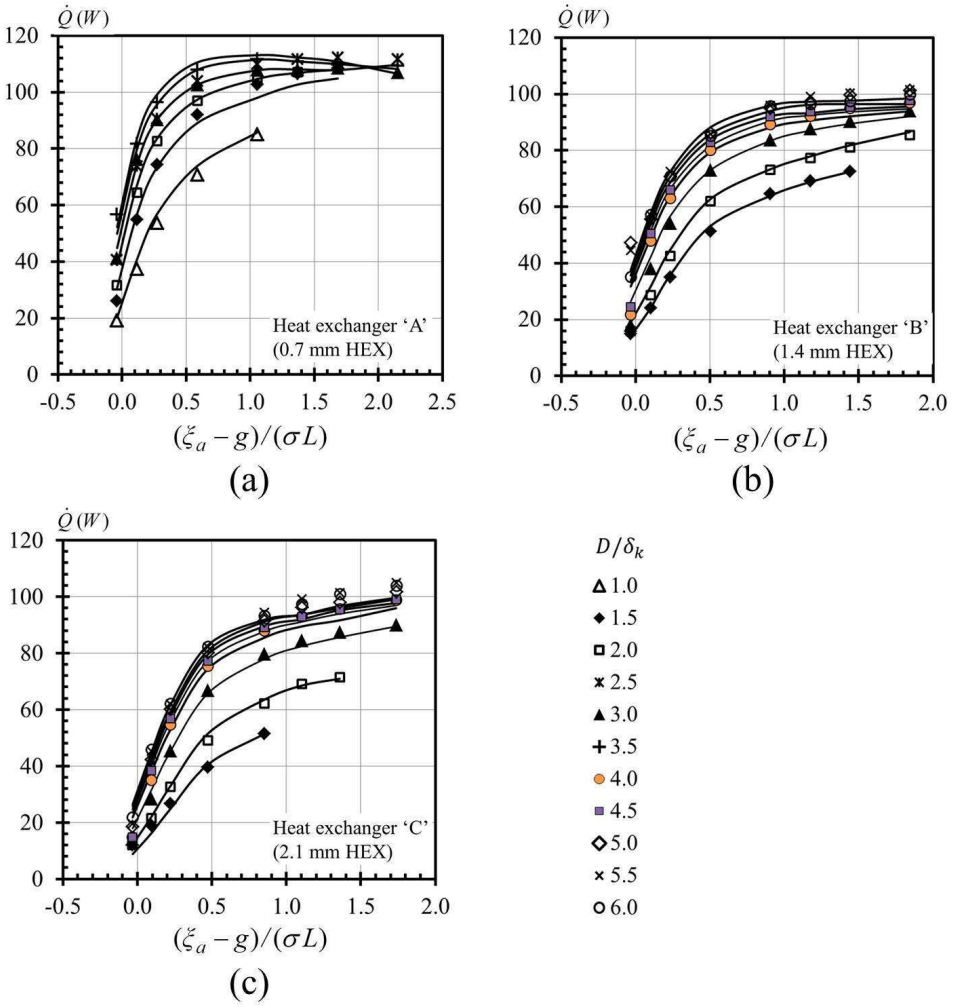


Figure 10: Dependence of heat transfer rates from experiments ($\dot{Q}_{exp}$)(symbols) and from the estimation ($\dot{Q}_{est}$)(lines) on $(\xi_a - g)/(\sigma L)$ and $D/\delta_\kappa$ for heat exchangers 'A' (a), 'B' (b) and 'C' (c), when $T_{h,i} = 80\,^\circ$C.

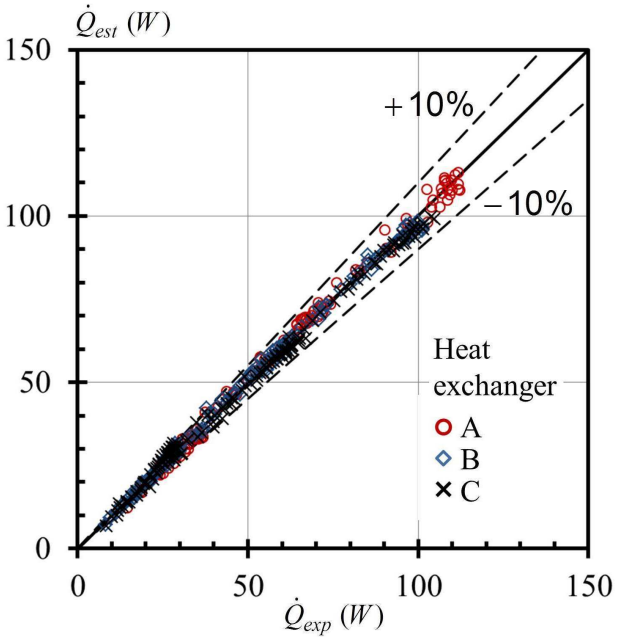


Figure 11: Heat transfer rate from experiment ($\dot{Q}_{exp}$) in comparison with the estimated values ($\dot{Q}_{est}$).

growth rate becomes lower for $(\xi_a - g)/(\sigma L) > 0.5$ and tends to be further reduced when $(\xi_a - g)/(\sigma L) > 1.5$. Similar trends can also be observed on heat exchangers 'B' (1.4 mm HEX) and 'C' (2.1 mm HEX), however, the reduction in the growth rate of the values of $Nu_{o,OSC}$ is much less.

The effect of $D/\delta_\kappa$ on $Nu_{o,OSC}$ was also investigated. Generally speaking, $Nu_{o,OSC}$ increases with $D/\delta_\kappa$. For heat exchangers 'B' and 'C', the maximal $Nu_{o,OSC}$ occur at $D/\delta_\kappa$ around 5.0  5.5. Regarding heat exchanger 'A', as the maximum $D/\delta_\kappa$ in the experiment is only 3.5, the peak of $Nu_{o,OSC}$ could not be clearly observed in this available range.

The Nusselt number obtained from measurements was compared with various models including, the RMS-Re model, the TASFE model, the modified-TASFE model, the boundary layer conduction model and the Valensi number integrated model. The comparison shows that these models constantly overestimate the gas side heat transfer coefficient of the heat exchangers of interest in oscillatory flow. Among these models, the boundary layer conduction model and the Valensi number integrated model provide predictions of heat transfer coefficient closer to experimental results.

A correlation between heat transfer effectiveness ($\epsilon$), and the normalized fin spacing ($D/\delta_\kappa$) and the normalized fin length $(\xi_a - g)/(\sigma L)$ was developed. The heat transfer effectiveness determined from the proposed correlation can be used to evaluate the heat transfer rate. Overall, the deviation between the estimated heat transfer rate and the heat transfer rate obtained from the measurements in current work is about 5.4% on average. It is expected that this correlation could be used for the design of thermoacoustic heat exchangers for alike heat exchangers in similar operating conditions.

## Acknowledgment

This work was financially supported by the EC-funded project "Thermoacoustic Technology for Energy Applications" under the 7th Framework Programme (FP7) (Grant Agreement No. 226415, Thematic Priority: FP7-ENERGY-2008-FET, Acronym: THATEA). The funding enabled the development of the experimental apparatus and the necessary instrumentation. The first author also gratefully acknowledges the financial support received from the Royal Thai Government and the University of Phayao, Thailand. The authors also wish to express their appreciation to the reviewers and editors for their very useful comments.

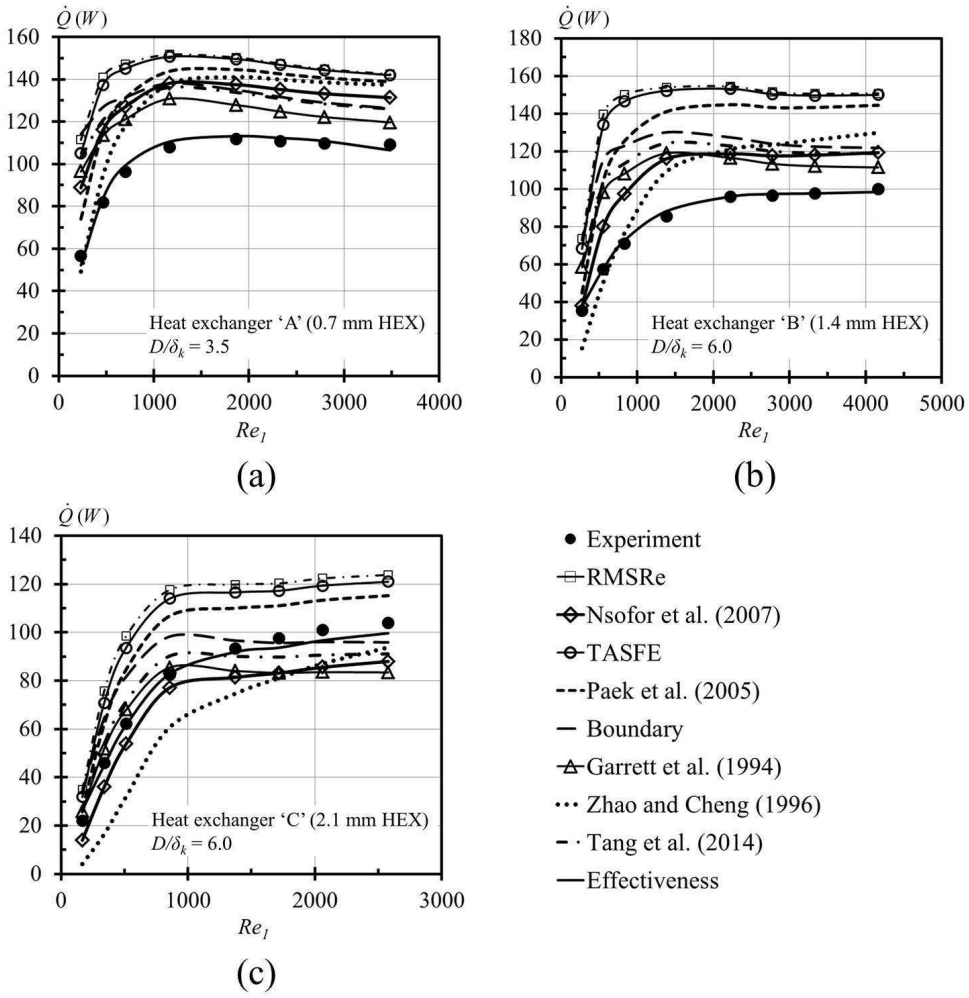


Figure 12: Estimated heat transfer rates compared with experimental results at selected conditions for heat exchanger 'A' (a), 'B' (b) and 'C' (c).

## References


[1] B. L. Minner, J. E. Braun, L. Mongeau, Optimizing the design of a thermoacoustic refrigerator, in: International Refrigeration and Air Conditionaing Conference, School of Mechanical Engineering, Purdue University, 1996, pp. 315–322.

[2] M. E. H. Tijani, J. C. H. Zeegers, A. T. A. M. de Waele, Design of thermoacoustic refrigerators, Cryogenics 42 (1) (2002) 49–57.

[3] A. S. Worlikar, O. M. Knio, Numerical study of oscillatory flow and heat transfer in a loaded thermoacoustic stack, Numerical Heat Transfer Part A Applications 35 (1) (1999) 49–65.

[4] E. Besnoin, O. M. Knio, Numerical study of thermoacoustic heat exchangers in the thin plate limit, Numerical Heat Transfer, Part A Applications 40 (5) (2001) 445–471.

[5] D. Marx, P. Blanc-Benon, Numerical simulation of stack-heat exchangers coupling in a thermoacoustic refrigerator, AIAA Journal 42 (7) (2004) 1338–1347.

[6] A. Piccolo, Heat transfer characteristics of parallel-plate thermoacoustic heat exchangers, in: Conference on Thermal and Environmental Issues in Energy Systems, ASME-ATI-UIT, 2010, p. 1331.

[7] A. Piccolo, Numerical computation for parallel plate thermoacoustic heat exchangers in standing wave oscillatory flow, International Journal of Heat and Mass Transfer 54 (21-22) (2011) 4518–4530.

[8] A. Piccolo, G. Pistone, Estimation of heat transfer coefficients in oscillating flows: The thermoacoustic case, International Journal of Heat and Mass Transfer 49 (9-10) (2006) 1631–1642.

[9] J. R. Brewster, R. Raspet, H. E. Bass, Temperature discontinuities between elements of thermoacoustic devices, Journal of the Acoustical Society of America 102 (6) (1997) 3355–3360.

[10] R. S. Wakeland, R. M. Keolian, Effectiveness of parallel-plate heat exchangers in thermoacoustic devices, Journal of the Acoustical Society of America 115 (6) (2004) 2873–2886.

[11] I. Paek, J. E. Braun, L. Mongeau, Characterizing heat transfer coefficients for heat exchangers in standing wave thermoacoustic coolers, Journal of the Acoustical Society of America 118 (4) (2005) 2271–2280.

[12] E. C. Nsofor, S. Celik, , X. Wang, Experimental study on the heat transfer at the heat exchanger of the thermoacoustic refrigerating system, Applied Thermal Engineering 27 (14-15) (2007) 2435–2442.

[13] K. Tang, J. Yu, T. Jin, Y. P. Wang, W. T. Tang, Z. H. Gan, Heat transfer of laminar oscillating flow in finned heat exchanger of pulse tube refrigerator, International Journal of Heat and Mass Transfer 70 (2014) 811–818.

[14] G. W. Swift, Thermoacoustics: a unifying perspective for some engines and refrigerators, Acoustical Society of America through the American Institute of Physics, Melville, NY, 2001.

[15] N. Cao, J. R. Olson, G. W. Swift, S. Chen, Energy flux density in a thermoacoustic couple, Journal of the Acoustical Society of America 99 (6) (1996) 3456–3464.

[16] G. W. Swift, Thermoacoustic engines, Journal of the Acoustical Society of America 84 (4) (1988) 1145–1180.

[17] F. P. Incropera, D. P. DeWitt, T. L. Bergman, A. S. Lavine, Introduction to Heat Transfer, John Wiley & Sons, 2006.

[18] W. Kamsanam, Development of experimental techniques to investigate the heat transfer processes in oscillatory flows, Doctor of philosophy, University of Leicester (2014).

[19] E. P. Rood, D. P. Telionis, Journal of fluids engineering policy on reporting uncertainties in experimental measurements and results, Journal of Fluids Engineering Transactions of the ASME 113 (3) (1991) 313–314.

[20] J. H. Kim, T. W. Simon, R. Viskanta, Journal-of-heat-transfer policy on reporting uncertainties in xxperimental measurements and results, Journal of Heat Transfer Transactions of the ASME 115 (1) (1993) 5–6.

[21] H. Coleman, W. Steele, Experimentation, validation, and uncertainty analysis for engineers, John Wiley & Sons, New Jersey, 2009.

[22] S. J. Kline, F. A. McClintock, Describing uncertainties in single-sample experiments, Mechanical Engineering 75 (1) (1953) 3–8.

[23] G. Mozurkewich, Heat transfer from transverse tubes adjacent to a thermoacoustic stack, Journal of the Acoustical Society of America 110 (2) (2001) 841–847.

[24] G. W. Swift, Analysis and performance of a large thermoacoustic engine, Journal of the Acoustical Society of America 92 (3) (1992) 1551–1563.

[25] B. Ward, J. Clark, G. W. Swift, Design Environment for Low-amplitude ThermoAcoustic Energy Conversion (DeltaEC), Version 6.3b11, Uers Guide, 2012.

[26] T. S. Zhao, P. Cheng, Oscillatory heat transfer in a pipe subjected to a laminar reciprocating flow, Journal of Heat Transfer, Transactions of the ASME 118 (3) (1996) 592–597.

[27] S. L. Garrett, D. K. Perkins, A. Gopinath, Thermoacoustic refrigerator heat exchangers: design, analysis and fabrication, Heat Transfer 1994, Proceedings 10th International Heat Transfer Conference 4 (1994) 375–380.